JOURNAL OF GEOPHYSICAL RESEARCH, VOL. 85, NO. C9, PAGES 4996–5002, SEPTEMBER 20, 1980

Optical Image and Laser Slope Meter Intercomparisons of High-Frequency Waves

S. C. LUBARD, J. E. KRIMMEL, AND L. R. THEBAUD

Areté Associates, Santa Monica, California 90403

D. D. EVANS AND O. H. SHEMDIN

Jet Propulsion Laboratory, Pasadena, California 91103

Spectral analyses of optical images of the ocean surface, obtained by the Riverside Research Institute digital video system, are presented and compared with wave data measured simultaneously by the Jet Propulsion Laboratory (JPL) Waverider-mounted laser slope meter. The image analyses, which incorporate several new ideas, provide two-dimensional wave number spectra of slope, covering wavelengths from 10 cm to 10 m. These slope spectra are converted to wave height spectra by a new technique which includes the effects of sky radiance gradients. Space-time spectra are also presented for waves whose frequencies are less than 2 Hz. The JPL slope frequency spectra are compared with image wave number spectra which have been converted to frequency spectra by use of the gravity wave dispersion relation. Results of comparisons between the frequency spectra obtained from the two different measurements show reasonable agreement for frequencies less than 3 Hz.

1. Introduction

In this paper we use optical image data to obtain quantitative two-dimensional spectral information about ocean wave slopes, and we present comparisons of these spectral results with coincident wave slope frequency spectra obtained from the Jet Propulsion Laboratory (JPL) Waverider-mounted laser slope meter [*Shemdin and Tober*, 1979]. The optical image data were taken in digital form at the National Ocean Systems Center (NOSC) Tower during the West Coast Experiment [*Shemdin*, 1977] with the Riverside Research Institute (RRI) digital video system (DVS) [*Jao*, 1976].

Figure 1 illustrates the experimental geometry used to obtain the optical image and laser slope meter data. The DVS was positioned approximately 18 m (depending on tide) above the ocean and operated at a depression angle of 30°. With its real-time digitization, computer control system, and zoom lens the DVS is a versatile instrument for obtaining optical image data in digital form.

The particular image formats and spatial and temporal sampling used in this experiment are given in Table 1. Two-dimensional frames of normalized intensity from both formats are digitally processed to obtain spatial spectra covering two decades of wave number. These spectra are converted to ocean wave height spectra with the use of sky gradient information inferred from the time-averaged ocean optical intensities. The large-scale B data (see Table 1), recorded at the higher temporal sampling rate, can also be used to obtain space-time spectra for waves with frequencies less than 2 Hz. Details on the spectral analysis of the optical image data and interpretation of the results for several cases are given in section 2.

Measurements of wave slope at a point were obtained with the fast response laser-optical detector developed at the University of Florida to facilitate studies of short surface waves. A complete description of this instrument is given by *Palm* [1975]. Temporal spectra for slopes in the optical look and cross-look directions are estimated from these measurements. A description of the analysis performed on the slope meter data and presentation of the spectral results are included in section 3.

In order to compare the image wave number spectra with the slope meter frequency spectra we utilize the gravity wave dispersion relation. We describe the conversion from wave number to frequency spectra in section 4 and present the results from the two measurements.

2. Optical Image Analysis and Results

Background

Optical image techniques (photographs) have been used for many years to characterize ocean surface waves. *Cox and Munk* [1954] used the variation of the glint-dominated irradiance on photographs to obtain the ocean slope probability density function as a function of wind speed. More recently, *Stilwell* [1969], *Stilwell and Pilon*, [1974], *Kasevich et al.* [1972], and *Kasevich* [1975] have presented techniques for using the spatial variations recorded on an ocean photograph that is illuminated by diffuse skylight to extract wave slope and wave height power spectral densities. In all these studies a Taylor series expansion of the general nonlinear dependence of measured irradiance on wave slope is used. In the Stilwell analysis, only the linear terms and nonuniform sky radiance are considered, while Kasevich considers the quadratic terms and also includes nonuniform sky effects. In the following paragraphs we develop the linear result in a form somewhat different from that given in the previous works and illustrate a convenient method for obtaining the actual sky gradient from the time-averaged ocean image data.

Modeling of the Image Data

The DVS image data are recorded in real time in digital form (counts) on magnetic tape. We assume that the DVS measurement $m(\mathbf{x}', t)$ at each pixel is related to the sea surface normal $\hat{n}(\mathbf{x}, t)$ (assuming that the altitude is much greater than

Paper number 80C0435.
0148-0227/80/080C-0435$01.00

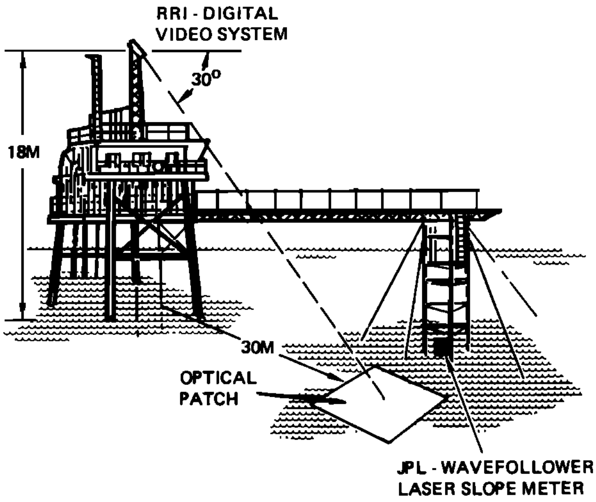

Fig. 1. Basic geometry for the intercomparison experiment.

the wave height) by

$$m(\mathbf{x}', t) = K(\mathbf{x}')[p_H\eta_H(\beta, \alpha; \hat{n})N_H(\beta, \alpha; \hat{n}) + \text{(vertical polarization term)}] + d(\mathbf{x}', t) \qquad (1)$$

where η_H is the horizontal Fresnel reflectivity, N_H is the horizontally polarized sky radiance (horizontal is defined with respect to the sea surface normal vector), p_H is the transmissivity for the horizontal polarization filter at the camera (if present), $K(\mathbf{x}')$ is the image system sensitivity, and $d(\mathbf{x}', t)$ is the fluctuating vidicon dark current noise. There is, of course, a mapping between the image pixel coordinate $\mathbf{x}'$ and the ocean coordinate $\mathbf{x}$. Figure 2 illustrates the reflection geometry and nomenclature.

The time average of m at each $\mathbf{x}'$ is formed and used to define a zero mean normalized measurement,

$$M(\mathbf{x}', t) \equiv \frac{m - \langle m \rangle}{\langle m \rangle - \langle d \rangle} \qquad (2)$$

where

$$\langle m \rangle - \langle d \rangle = K(\mathbf{x}')[p_H < \langle \eta_H N_H \rangle + p_V \langle \eta_V N_V \rangle] \qquad (3)$$

The $\langle d \rangle$ term is measured at each pixel by averaging 100 frames of data obtained with the camera shutter closed.

We simplify this presentation by dropping the vertical polarization term. This is valid for the linear analysis which follows, if the sky radiance is unpolarized ($N_H = N_V$) and a horizontal camera polarizer is used (as is the case for these data). Equation (2) becomes

$$M(\mathbf{x}', t) = \frac{\eta N - \langle \eta N \rangle}{\langle \eta N \rangle} \qquad (4)$$

where we have dropped the subscript H. We separately expand the functions η and N in Taylor series of the slope components ϵ_1 (look) and ϵ_2 (cross look), and keeping only the first-order terms, we obtain

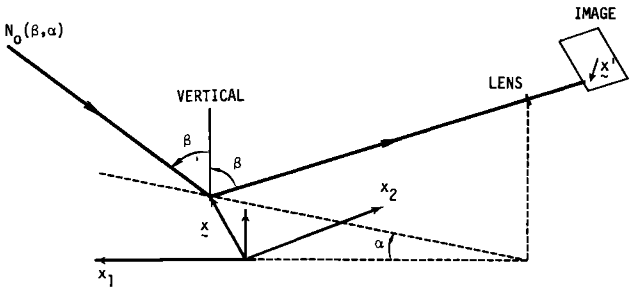

Fig. 2. Image analysis geometry and notation.

$$M(\mathbf{x}', t) = \left[-\left(\frac{1}{\eta_0} \frac{\partial \eta_0}{\partial \beta} \right) - \left(\frac{2}{N_0} \frac{\partial N_0}{\partial \beta} \right) \right] \epsilon_1 + \left[-2 \cot \beta \left(\frac{1}{N_0} \frac{\partial N_0}{\partial \alpha} \right) \right] \epsilon_2 \qquad (5)$$

The time-averaged ocean data can be conveniently used to obtain actual values for N_0 (β, α) and its first derivatives if the data cover a sufficient field of view. Through first order we have (from (3))

$$\langle m(x', t) \rangle - \langle d \rangle = K(\mathbf{x}')\eta_0(\beta)N_0(\beta, \alpha) \qquad (6)$$

where $K(\mathbf{x}')$ is independently determined up to an overall scale factor and η_0 at each pixel is given by

$$\eta_0(\beta) = \frac{\sin^2 [\beta - \sin^{-1} (\sin \beta/1.34)]}{\sin^2 [\beta + \sin^{-1} (\sin \beta/1.34)]} \qquad (7)$$

where 1.34 is the index of refraction for water.

Equation (5) displays the linear relation between the normalized instantaneous measurement at each camera pixel and the ocean slope components. We will neglect the slow variation of the coefficients over the image field of view.

Image Data Analysis

We utilize the previous analysis as the basis for the image data spectral analysis. The particular cases initially selected for investigation are given in Table 2. Note that OW65 and OW73 are larger-scale B data types, while OW71 is the small-scale A data type (see Table 1). We use the time average of the data over several minutes to normalize the data for each frame. A two-dimensional spectral package developed at Areté [*Nelson and Marquez,* 1975] is then utilized to obtain the sample spatial power spectrum for each of 99 uniformly time-sampled frames of data covering the data record. These sample spectra are then ensemble-averaged to obtain a final spatial spectrum. Assuming that the individual spectral estimates are independent, these ensemble-averaged estimates are within ±0.6 dB of the mean at the 90% confidence level.

TABLE 1. Optical Image Data Formats

Data Type	Patch Size (Look × Cross Look), m	Field of View, deg	Frame Dimension (Look × Cross Look), pixels	Frame Time, s	Data Length, Frames
A (small scale)	3.1 × 0.5	2.5 × 0.9	200 × 70	0.57	1000
B (large scale)	11.8 × 6.0	9.4 × 9.4	80 × 80	0.29 or 0.57	2000

The camera depression angle is 30°, the camera altitude is 18, and the camera polarizer is horizontal.

TABLE 2. Image Cases Analyzed

Case	Date	Start Time	Data Type	Sky	Look Azimuth, deg	Wind Direction (From), °T	Wind Speed, kn (m/s)	Frame Time, s	Total No. of Frames
OW65	April 5	1325	large	clear	340	325	15 (7.5)	0.29	1000
OW71	April 6	1106	small	overcast	240	320	15 (7.5)	0.57	2000
OW73	April 6	1237	large	overcast	240	325	15 (7.5)	0.57	2000

JPL slope meter data are for April 6, starting at 1240 hours.

Figure 3 shows the resultant spatial spectrum for OW73. Contours of equal spectral density separated by $2\frac{1}{2}$ dB are presented. Because the input data are real, the spectrum is diagonally symmetric. The notch in the spectrum apparent in Figure 3 is predicted by (5) to lie along the line

$$k_1 = \left[\frac{2\cot\beta[(1/N_0)(\partial N_0/\partial\alpha)]}{-[(1/\eta_0)(\partial\eta_0/\partial\beta)] - [(2/N_0)(\partial N_0/\partial\beta)]}\right] k_2 \qquad (8)$$

The wave height spectrum $P_\zeta(\mathbf{k})$ is related to the measured spectrum $P_M(\mathbf{k})$ by

$$P_M(\mathbf{k}) = \left\{\left[-\left(\frac{1}{\eta_0}\frac{\partial\eta_0}{\partial\beta}\right) - \left(\frac{2}{N_0}\frac{\partial N_0}{\partial\beta}\right)\right] k_1 + \left[-2\cot\beta\left(\frac{1}{N_0}\frac{\partial N_0}{\partial\alpha}\right)\right] k_2\right\}^2 P_\zeta(\mathbf{k}) \qquad (9)$$

In order to obtain a quantitative wave height spectrum we require values for the sky gradients. These can be obtained from the average ocean data for this case (since the field of view is 9.4° in each direction) with the aid of (6) and (7). The result for OW73 is illustrated in Figure 4, which shows contours of constant values of N_0 (β, α) normalized to a mean value of 1. A least squares plane fit to this case gives

$$\left(\frac{1}{N_0}\frac{\partial N_0}{\partial\beta}\right) = -0.59 \quad \text{rad}^{-1}$$
$$\left(\frac{1}{N_0}\frac{\partial N_0}{\partial\alpha}\right) = -0.90 \quad \text{rad}^{-1} \qquad (10)$$

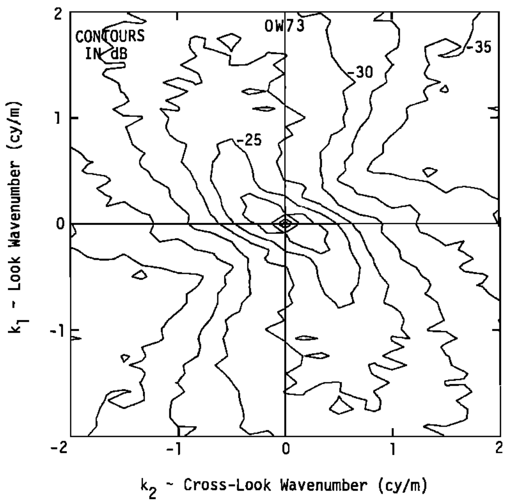

Fig. 3. OW73 image spatial spectrum obtained by averaging 99 sample spectra from frames 11.4 s apart: 0 dB = 1 (normalized intensity)^2/(cpm)^2.

This implies a notch in the measured spectrum at an angle of 25° from the positive k_2 axis, in good agreement with Figure 3.

The wave height spectrum for OW73 obtained by the use of (9) is shown in Figure 5. The invisible region is taken as being approximately ±20° around the notch line.

Figures 6 and 7 show results analogous to those in Figures 3 and 5 for the OW65 case. This case is seen to have less cross-look sky gradient than the previous case. It is also useful to consider a space-time spectrum of the measurements for this case because of its higher frame rate. We obtain this by averaging each frame of normalized data in the cross-look direction (thus effectively filtering waves that are not in the look direction) and using the Areté two-dimensional spectral routine. The resulting space-time spectrum for OW65 is presented in Figure 8. Statistical stability for this case has been obtained by averaging over boxes of 11 elemental frequency bins, and by ensemble averaging over four distinct data segments. Contours of equal power spectral density are presented, and the dispersion curve is included for reference. Most of the energy lies along this curve in a direction toward the camera, which also corresponds to that of the wind vector.

Finally, Figure 9 displays the analysis results for the two-dimensional spatial wave height spectrum in the small-scale OW71 case. The sky gradients were taken as zero for this case.

In order to interpret the quantitative optical image spectral results we must discuss two issues. First, in transforming the equally spaced optical image data we have neglected the distortion induced by the nonlinear terms in the mapping between the image coordinate $\mathbf{x}'$ and the ocean coordinate $\mathbf{x}$. In omitting these terms we smear the actual spectrum over an interval in $\mathbf{k}$ space. For our large-size patch (which is the worst

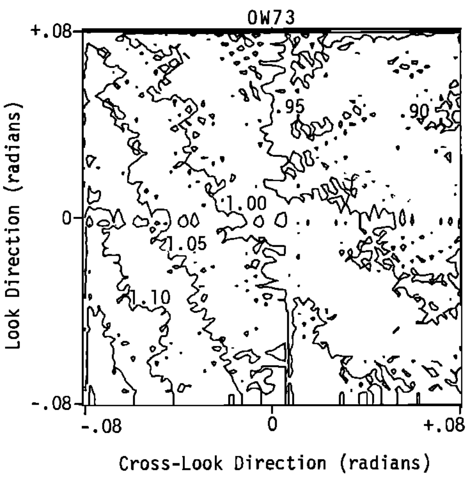

Fig. 4. OW73 average normalized sky radiance. Angles are measured from the camera axis.

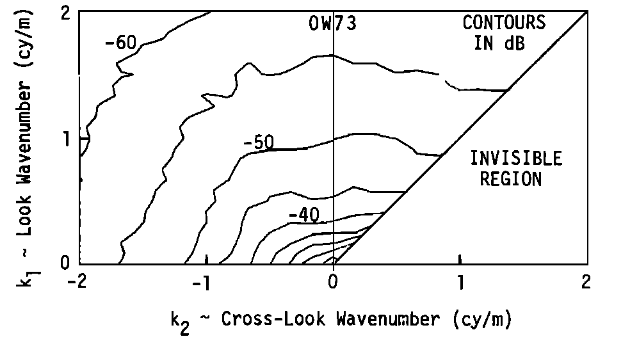

Fig. 5. OW73 wave height spatial spectrum: 0 dB = 1 $m^2/(cpm)^2$.

case) an estimate shows that the smearing width in the k domain is approximately 14%. This smearing thus introduces a bias into the measured slope spectra (Figures 3 and 6) of less than 1 dB.

We call the second, more subtle issue 'tilt distortion.' For our data we expect the entire area of the patch to be tilted randomly for every frame by longer waves (swell). Since we are looking at the ocean at a relatively low depression angle, this tilt will distort the wave fronts of the smaller waves and thus distort an optically measured spectrum. Quantitative modeling performed at Areté (L. Thebaud, unpublished data, 1980) indicates that the relative magnitude of this effect on the spatial spectrum is of the order of $\tan^2 \beta \langle \epsilon^2 \rangle$. This result leads us to expect the 'tilt' effect to be negligible for these data.

We will use the wave number spectra presented in Figures 5, 7, and 9 to compare with the results of the laser slope meter frequency spectra.

3. Point Wave Slope Measurements and Analysis

Instrumentation

A high-response laser-optical wave slope detector developed at the University of Florida was used to facilitate studies

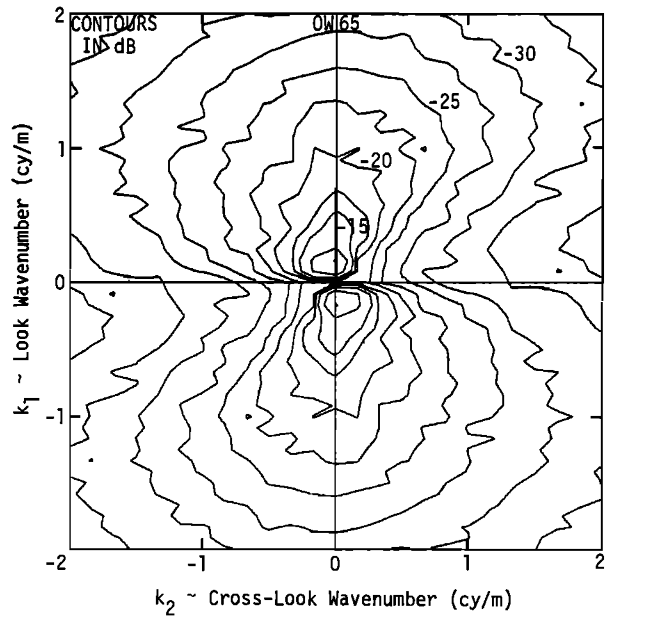

Fig. 6. OW65 image spatial spectrum obtained by averaging 99 sample spectra from frames 5.8 s apart: 0 dB = 1 (normalized intensity)^2/(cpm)^2.

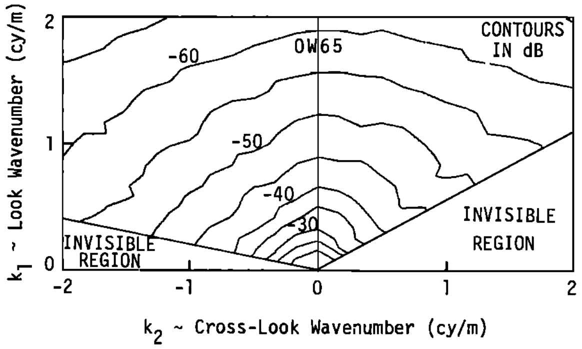

Fig. 7. OW65 wave height spectrum: 0 dB = 1 $m^2/(cpm)^2$.

of short surface waves. The earlier version of this sensor was described by *Tober et al.* [1973], and an improved model was described by *Palm* [1975]. The most recent instrument model used in both wave tank and field studies is shown in Figure 10*a*. A vertical laser beam originating underwater is used. The beam is bent by refraction at the surface when waves are present. The deflection angle is related to the surface wave slope and is detected by an optical receiver with a photodiode, which determines the position of the deflected beam. The response of the sensor is limited by the size of the laser beam spot on the water surface. A notable design feature of the laser-optical instrument is its insensitivity to mean water surface displacements to within ±30 cm. The instrument is especially suitable for the study of modulation of short waves by long waves provided that the long-wave amplitude does not exceed 30 cm. However, this amplitude constraint is stringent for field studies, where 1.0-m wave amplitudes often occur. To offset such a limitation, the laser-optical device was mounted on a wave-following platform (Waverider) capable of tracking long ocean waves with frequencies less than 0.3 Hz to within an accuracy of ±10 cm. The wave-follower design specifications and capabilities were reported by *Shemdin and Tober* [1979]. Thus the laser-optical instrument, when mounted on the Waverider, allows measurement of short waves with amplitudes of ±20 cm and their modulation by long ocean waves. The combined apparatus, shown in Figure 10*b*, was deployed at the NOSC Tower in water of 18-m depth. We now consider the analysis of the acquired data.

Analysis

The laser-optical device made four simultaneous voltage measurements at a rate of 200 Hz. These voltages in turn provided the normal vector of the ocean surface above the laser at each instant in time. More specifically, this transformation

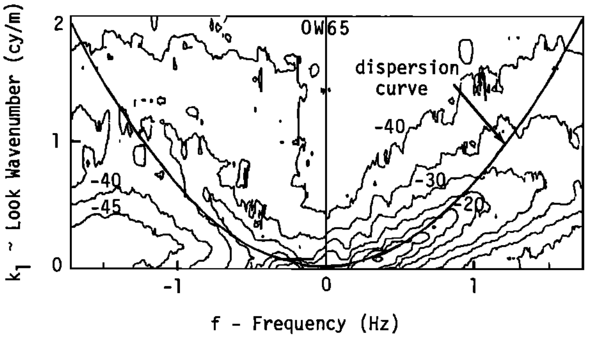

Fig. 8. OW65 cross-look averaged space-time spectrum. Energy in the right half is moving toward the camera.

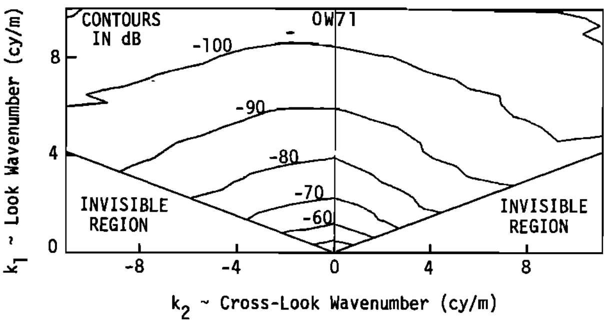

Fig. 9. OW71 image spectrum: 0 dB = 1 $m^2/(cpm)^2$.

was made via a third-order polynomial least squares fit of actual calibration data. For each direction $\hat{r}$ of interest we then calculated the slope of the sea surface in the $\hat{r}$ direction and in a direction perpendicular to $\hat{r}$. In Figures 11*a* and 11*b* we show 5-s-long time histories of slope from the data set obtained simultaneously with the image data on April 6, 1977. Figure 11*a* is for the 240° azimuth slope component, and Figure 11*b* is for the 150° azimuth slope component. It should be mentioned that it was not uncommon for several percent of the data to be clearly nonphysical. Such points were randomly scattered, and we replaced them with the value preceding them. These bad points do not significantly degrade our results.

We obtain an estimate of frequency spectra from these data by ensemble averaging 21 individual spectra taken over 1-hour duration. Each individual spectrum is computed from a segment 5.12 s long. Our statistical uncertainty for these spectral estimates is approximately ±1.3 dB relative to the mean at the 90% confidence level. It is important to point out that we have additional uncertainty due to the long gravity waves modulating the wavelength, amplitude, direction, and encounter frequency of short waves. Air-sea interaction also contributes to this phenomenon, especially in the presence of wind. The ensemble averaging tends to eliminate some of the effects of the long-wavelength modulation. A spectrum for the 240° azimuth slope component is given in Figure 11*c*. The high-frequency limit in the plot is 100 Hz, whereas the instrument itself has a flat response up to 80 Hz.

4. Image and Slope Meter Intercomparisons

In order to compare the image spatial spectra with the slope frequency spectra we will convert the two-dimensional wave height spatial spectra to frequency. We use the deepwater gravity wave dispersion relation

$$\omega^2 = gk \tag{11}$$

valid for wavelengths of >5 cm. The required conversion formulas become [*Phillips*, 1977]

$$P_\zeta(\omega) = \frac{\omega^3}{2\pi g^2} \int_{-\pi}^{\pi} P_\zeta(k, \theta)\, d\theta \tag{12}$$

$$P_{\epsilon_1}(\omega) = \frac{\omega^7}{2\pi g^4} \int_{-\pi}^{\pi} P_\zeta(k, \theta) \cos^2\theta\, d\theta \tag{13}$$

$$P_{\epsilon_2}(\omega) = \frac{\omega^7}{2\pi g^4} \int_{-\pi}^{\pi} P_\zeta(k, \theta) \sin^2\theta\, d\theta \tag{14}$$

where θ is the angle measured from the look direction (k_1 axis). Extrapolation is used to derive the contribution to these integrals for the invisible regions indicated in Figures 5, 7, and 9. The spectral levels from these formulas are such that the integral over all frequencies (positive and negative) in hertz gives the variance. This is the convention which is used for all the spectra presented in this paper.

Figure 12 presents the results for $P_\zeta(\omega)$ from the image data compared with the model spectrum from *Phillips* [1977]. This simple model is included as a convenient reference, not as a necessarily realistic model of the ocean. Here the agreement is reasonable for frequencies less than 3 Hz; however, for the higher frequencies the image data integrals fall off more rapidly than the model spectrum. No wave height information was available from the slope meter.

Figures 13*a* and 13*b* present the quantitative comparisons

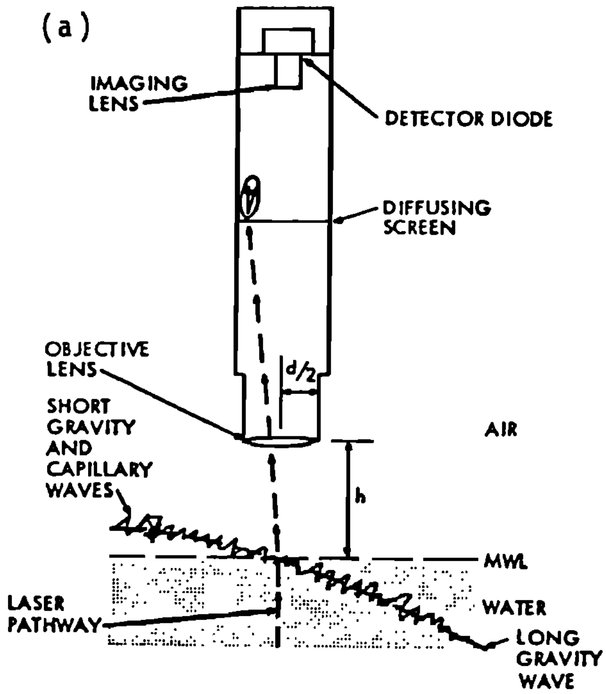

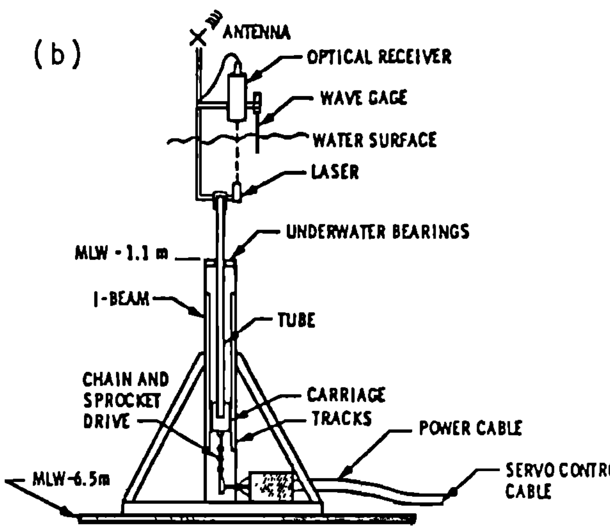

Fig. 10. Laser-optical device for detection of short wave slopes. (*a*) Laser slope meter. (*b*) Combined receiver and Waverider.

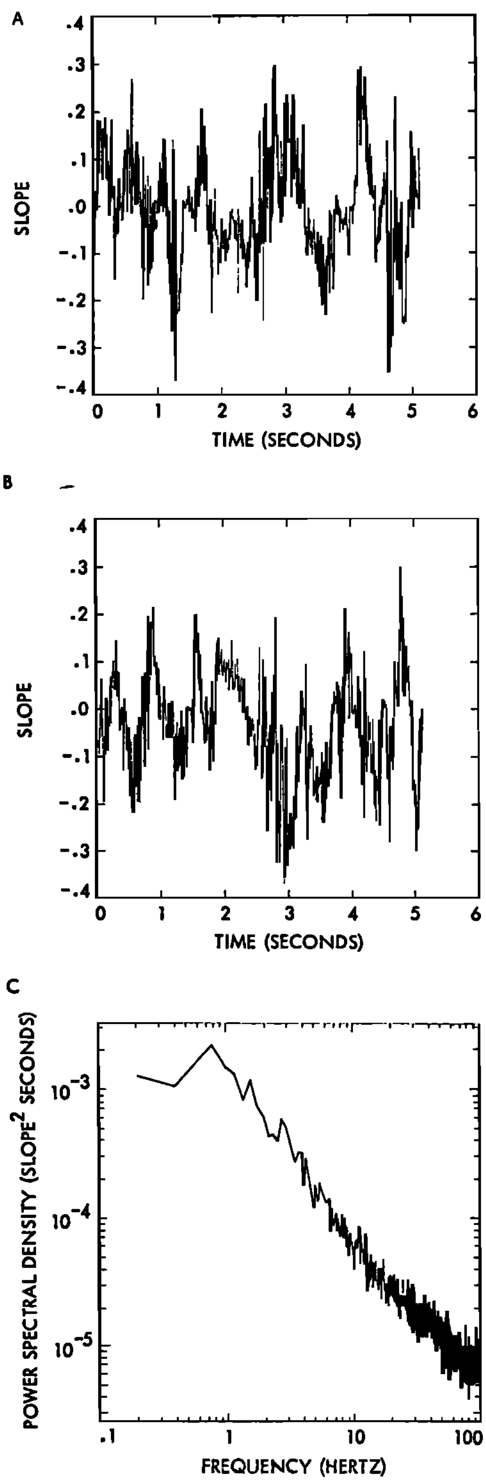

Fig. 11. Slope time history. (*a*) Sample 240° from north. (*b*) Sample 150° from north. (*c*) Power spectral density 240° from north.

between the image frequency spectra and the simultaneous slope meter spectra for the slope components in approximately the wind and crosswind directions. The image results from cases OW73 and OW71 are for data obtained simultaneously with the slope meter data, while the OW65 result is for the same wind speed but a different day. Also shown in these figures, for reference only, is the symmetric model slope spectrum from *Phillips* [1977]. The quantitative agreement between the different measurements for the slope component in

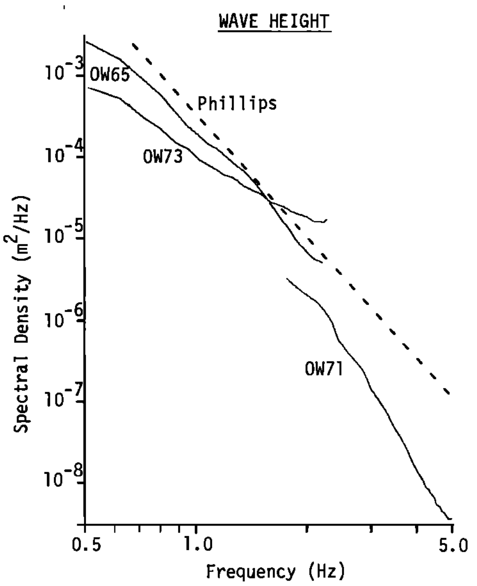

Fig. 12. Wave height spectral density versus frequency derived from the image data.

the wind direction is good for frequencies less than 3 Hz. The crosswind slope component results for the OW73 image data are somewhat lower than the slope meter data at frequencies less than 1 Hz. The OW71 image results for both slope com-

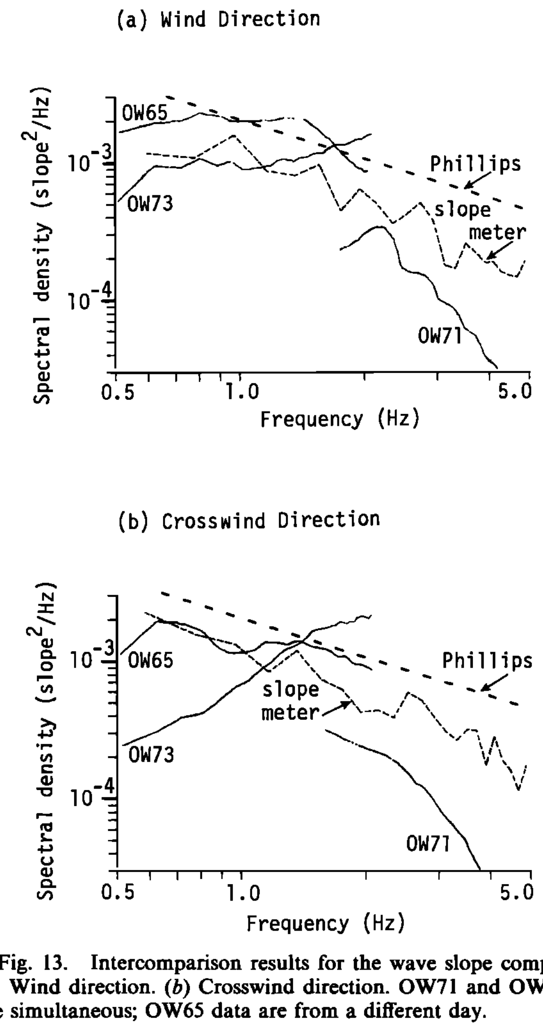

Fig. 13. Intercomparison results for the wave slope components. (*a*) Wind direction. (*b*) Crosswind direction. OW71 and OW73 data are simultaneous; OW65 data are from a different day.

ponents at frequencies greater than 3 Hz (OW71 allows output at higher frequencies because of its finer spatial sampling) decrease more rapidly with frequency than the slope meter data.

5. Discussion and Summary

Quantitative comparisons of ocean slope frequency spectra generated by using simultaneous optical image and point slope meter data have been presented for the first time. In addition, quantitative two-dimensional wave height spectra covering wavelengths from 10 m to 10 cm for a wind speed of 15 kn (7.5 m/s) have been generated from the optical image data. The comparisons cover the range of frequencies from 0.5 to 5 Hz.

The agreement of the two data types for frequencies less than 3 Hz is generally within 3 dB. Since the purely statistical uncertainty in each measurement has been estimated as about 1 dB, the data show evidence of some systematic errors. For example, the image-derived spectra at frequencies greater than 3 Hz fall off more rapidly than the slope meter predictions. This disagreement at the higher frequencies may be due to these shorter waves experiencing a large temporal Doppler shift tending to displace to higher frequency the energy of waves at a given wave number. Further work on this issue and comparisons for additional cases are now being performed.

Acknowledgments. The authors would like to acknowledge the support of Riverside Research Institute and especially Marvin King, Jen King Jao, and William Hendrickson in acquiring and supplying the optical image data used in these analyses. We would also like to acknowledge the support of John Wartman of Areté Associates, who aided in the development of the optical data analysis software used in this paper.

References

Cox, C., and W. Munk, Measurements of the roughness of the sea surface from photographs of the sun's glitter, *J. Opt. Soc. Amer., 44,* 838–850, 1954.

Jao, J. K., Digital video system characterization, *Rep. T-4/342-3-10,* Riverside Res. Inst., New York, June 1976.

Kasevich, R. S., Directional wave spectra from daylight scattering, *J. Geophys. Res., 80,* 4535–4541, 1975.

Kasevich, R. S., C. H. Tang, and S. W. Hendriksen, Analysis and optical processing of sea photographs for energy spectra, *IEEE Trans. Geosci. Electron., GE-10,* 51–58, 1972.

Nelson, K. W., and R. D. Marquez, Two dimensional time series analysis subroutine package ALL2D, memorandum, Areté Ass., Santa Monica, Calif., Oct. 7, 1975.

Palm, C. S., An instrument to measure the two dimensional wave slope spectrum of ocean capillary waves, Ph.D. dissertation, Univ. of Fla., Gainesville, 1975.

Phillips, O., *Dynamics of the Upper Ocean,* 2nd ed., Cambridge University Press, New York, 1977.

Shemdin, O., West Coast Experiment test plan, technical report, Jet Propul. Lab., Pasadena, Calif., March 1977.

Shemdin, O. H., and G. Tober, Surface followers, in *Air-Sea Interaction: Instruments and Methods,* chap. 33, Plenum, New York, 1979.

Stilwell, D., Directional energy spectra of the sea from photographs, *J. Geophys. Res., 74,* 1974–1986, 1969.

Stilwell, D., and R. O. Pilon, Directional spectra of surface waves from photographs, *J. Geophys. Res.,79,* 1277–1284, 1974.

Tober, G., R. C. Anderson, and O. H. Shemdin, Laser instrument for detecting water ripple slopes, *Appl. Opt., 12*(4), 788–794, 1973.

(Received August 20, 1979;
revised December 13, 1979;
accepted December 18, 1979.)